ROSETTA RADIO SCIENCE INVESTIGATIONS (RSI)

MARTIN PÄTZOLD[1,*], BERND HÄUSLER[2], KAARE AKSNES[3], JOHN D. ANDERSON[4], SAMI W. ASMAR[4], JEAN-PIERRE BARRIOT[5], MICHAEL K. BIRD[6], HERMANN BOEHNHARDT[7], WERNER EIDEL[2], EBERHARDT GRÜN[8], WING H. IP[9], ESSAM MAROUF[10], TREVOR MORLEY[11], FRITZ M. NEUBAUER[1], HANS RICKMAN[12], NICOLAS THOMAS[13], BRUCE T. TSURUTANI[4], MAX K. WALLIS[14], N. C. WICKRAMASINGHE[14], EIRIK MYSEN[3], OYSTEIN OLSON[3], STEFAN REMUS[2], SILVIA TELLMANN[1], THOMAS ANDERT[1], LUDMILA CARONE[1], MARKUS FELS[1], CHRISTINA STANZEL[1], IRIS AUDENRIETH-KERSTEN[1], ALEXANDER GAHR[1], ANNA-LIANE MÜLLER[1], DUSAN STUPAR[1] and CHRISTINA WALTER[1]

[1]*Institut für Geophysik und Meteorologie, Universität zu Köln, Köln, Germany*
[2]*Institut für Raumfahrttechnik, Universität der Bundeswehr München, Neubiberg, Germany*
[3]*Institute for Theorectical Astrophysics, University of Oslo, Oslo, Norway*
[4]*Jet Propulsion Laboratory, California Institute of Technology, Pasadena, California, USA*
[5]*GRGS/GTP, CNES, Toulouse, France*
[6]*Argelander Institut für Astronomie, Universität Bonn, Bonn, Germany*
[7]*Max-Planck-Institut für Sonnensystemforschung, Katlenburg-Lindau, Germany*
[8]*Max-Planck-Institut für Kernphysik, Heidelberg, Germany*
[9]*Institute of Astronomy, National Central University, Chung-Li, Taiwan*
[10]*Dept. of Electrical Engineering, San Jose State University, San Jose, California, USA*
[11]*ESA-ESOC, Darmstadt, Germany*
[12]*Astronomiska Observatoriet, University of Uppsala, Uppsala, Sweden*
[13]*Physikalisches Institut, Universität Bern, Bern, Switzerland*
[14]*School of Mathematics, University of Wales, Cardiff, UK*
*(*Author for correspondence: E-mail: paetzold@geo.uni-koeln.de)*

(Received 22 March 2006; Accepted in final form 13 November 2006)

Abstract. The Rosetta spacecraft has been successfully launched on 2nd March 2004 to its new target comet 67 P/Churyumov-Gerasimenko. The science objectives of the Rosetta Radio Science Investigations (RSI) experiment address fundamental aspects of cometary physics such as the mass and bulk density of the nucleus, its gravity field, its interplanetary orbit perturbed by nongravitational forces, its size and shape, its internal structure, the composition and roughness of the nucleus surface, the abundance of large dust grains, the plasma content in the coma and the combined dust and gas mass flux. The masses of two asteroids, Steins and Lutetia, shall be determined during flybys in 2008 and 2010, respectively. Secondary objectives are the radio sounding of the solar corona during the superior conjunctions of the spacecraft with the Sun during the cruise phase.

The radio carrier links of the spacecraft Telemetry, Tracking and Command (TT&C) subsystem between the orbiter and the Earth will be used for these investigations. An Ultrastable oscillator (USO) connected to both transponders of the radio subsystem serves as a stable frequency reference source for both radio downlinks at X-band (8.4 GHz) and *S*-band (2.3 GHz) in the one-way mode. The simultaneous and coherent dual-frequency downlinks via the High Gain Antenna (HGA) permit separation of contributions from the classical Doppler shift and the dispersive media effects caused by the motion of the spacecraft with respect to the Earth and the propagation of the signals through the dispersive media, respectively.

Space Science Reviews (2007) 128: 599–627
DOI: 10.1007/s11214-006-9117-7
© Springer 2007

source: https://doi.org/10.48350/25372 | downloaded: 17.4.2024

The investigation relies on the observation of the phase, amplitude, polarization and propagation times of radio signals transmitted from the spacecraft and received with ground station antennas on Earth. The radio signals are affected by the medium through which the signals propagate (atmospheres, ionospheres, interplanetary medium, solar corona), by the gravitational influence of the planet on the spacecraft and finally by the performance of the various systems involved both on the spacecraft and on ground.

Keywords: Rosetta, comets, 67 P/Churyumov-Gerasimenko, radio-science

1. Introduction

Initially conceived as an exploratory tool, radio science techniques have provided considerable knowledge of the atmospheres and gravity of the planets – some of which was originally unanticipated. Radio Science techniques are applied to the study of planetary and cometary atmospheres, planetary rings and surfaces, and gravity, as well as the solar corona. Much of our current knowledge of these subjects has been based on radio science observations.

Early missions incorporating radio science investigations included the Mariners, Pioneers, and Viking, as well as Soviet projects. Examples of recent and current experiments include those conducted with Voyager (Eshleman *et al*., 1977; Tyler, 1987), Ulysses (Bird *et al*., 1994; Pätzold *et al*., 1995), Giotto (Pätzold *et al*., 1991a,b, 1993), Galileo (Howard *et al*., 1992), Magellan (Tyler *et al*., 1991), Mars Global Surveyor (Tyler *et al*., 2001), Cassini (Kliore *et al*., 2002), Huygens (Bird *et al*., 2005), Mars Express (Pätzold *et al*., 2004, 2006), Venus Express (Häusler *et al*., 2006) and Pluto "New Horizons" (Stern and Spencer, 2003).

Radio science investigations fall into three broad categories of observation: gravity, propagation, and bistatic radar.

Gravity: When the radio path is well-clear of occulting material, the spacecraft can be treated as a classical 'test particle' falling in the gravity field of the body system. This type of experiment is optimized when the component of its change in velocity is along the line-of-sight to the tracking station, thus allowing a measurement of a gravity-induced Doppler effect. The spacecraft motion causing the Doppler shift is in response to the variations in mass distribution within a planet or its satellites. This is a classical physics laboratory experiment carried out on planetary scales. Our global knowledge of Earth's gravity field comes from such studies (e.g. Tapley *et al*., 2005). The only information on the gravity field of Mercury is based on the three flybys of Mariner 10 (Anderson *et al*., 1987). Similarly, recent observational inferences as to the internal structures of the Galilean satellites (among others, the subsurface ocean on Europa) are based on the perturbations of the trajectory of Galileo spacecraft during close flybys (Anderson *et al*., 1992, 1997, 2004). A precise determination of the total mass of Uranus and Neptune from the Voyager 2 flybys (Tyler *et al*., 1986) has led to the conclusion that there is no need for a 'Planet X' to explain the orbits of these bodies (Standish, 1993). The method has

been extended to small bodies as well, for example in the mass determination of the asteroid Mathilde (Yeomans *et al*., 1997), the gravity field of the asteroid Eros (Konopliv *et al*., 2002) and the Stardust flyby at comet P/Wild-2 in 2004 (Anderson *et al*., 2003, 2004). Techniques similar to those used for asteroids shall be applied for a precise determination of the masses of Mars moons Phobos and Deimos which are planned with Mars Express during its close encounters (Pätzold *et al*., 2006), and with Rosetta during its flybys at the asteroids Steins and Lutetia in 2008 and 2010, respectively.

Propagation: When the trajectory of the spacecraft carries it behind the planet as seen from Earth, the spacecraft is occulted by the planet's atmosphere. A radio signal propagating from the spacecraft to a ground station will travel through the ionosphere and the neutral atmosphere prior to being blocked by the planetary surface. The occultation entry sequence is repeated in reverse order upon emergence of the spacecraft from behind the planet. During an occultation event, the refractive index of the gases in the ionosphere and atmosphere alter the characteristics of the propagating radio wave. The method can be applied to planets, moons with atmospheres, cometary comae and can even be extended to any one of several separable 'atmospheres' including planetary rings and magnetospheres, as well as the relativistic gravitational effects (Eshleman, 1973). In conducting such observations the geometry and other experimental conditions must be controlled so that the only significant unknown factors are the properties of the medium along the radio path.

Bistatic radar: Oblique incidence scattering investigations using propagation paths between spacecraft, a planetary surface, and an Earth station, can be used to explore the surface properties through study of the microwave scattering function (Fjeldbo, 1964). Such investigations are referred to 'bistatic radar' since the transmitter and receiver are separated by significant angular distances or ranges. The first such experiment in space was conducted with Luna-11 in August 1966 to study the surface of the moon (Yakovlev and Efimov, 1966). The oblique scattering geometry afforded by the Lunar Orbiter-1 spacecraft, which orbited the moon in October 1966, provided the signal source for the first US experiment (Tyler *et al*., 1967). Recordings of signals transmitted to Earth by Explorer 35 also contained echos of the transmissions from the lunar surface (Tyler, 1968). By happenstance, the plane of the spacecraft spin axis and the antenna polarization during these recordings made it possible to measure the Brewster angle of the lunar crust. An unambiguous value was found for the relative dielectric constant of lunar soil between 2.9 and 3.1, thereby confirming that a future moon surface lander would be on firm ground. Bistatic radar experiments are performed on a routine basis with Mars Express (Simpson *et al*., 2006) and first observations have been performed with Venus Express in mid 2006 (Häusler *et al*., 2006).

Radio science experiments do not have a dedicated instrument on board the spacecraft but make use of the radio subsystem, which is primarily responsible for communication between the spacecraft and the ground stations on Earth.

The Rosetta radio subsystem is specially equipped with an Ultra-Stable Oscillator (USO), which significantly improves the sensitivity and accuracy of the measurements.

The launch cancellation of the Rosetta-Wirtanen mission in January 2003 resulted in a 13-month launch delay and the selection of a new target comet: 67 P/Churyumov-Gerasimenko. With a new final destination, Rosetta was successfully launched on 2 March 2004 and precisely injected into the desired interplanetary transfer orbit. The new mission includes three Earth flybys, one Mars flyby and possibly two asteroid flybys at Steins and Lutetia in 2008 and 2010, respectively, which were made feasible by the fuel saved from precise orbit injection and correction maneuvers. The arrival at the comet will be in mid 2014 with operations being conducted during the inbound orbital leg until perihelion in mid 2015.

The Rosetta Radio Science Investigations (RSI) experiment has identified primary and secondary science objectives at the comet, the asteroids flybys and during cruise. The primary science objectives are divided into categories

- cometary gravity field investigations,
- comet nucleus investigations,
- cometary coma investigations
- asteroid mass and bulk density

As a secondary science objective, RSI will perform coronal sounding experiments during the cruise phase solar conjunctions.

2. Current Knowledge of Relevant Physical Parameters of the Target Comet 67 P/Churyumov-Gerasimenko

The most important physical parameters of the nucleus of 67 P/Churyumov-Gerasimenko for the measurement sensitivity and accuracy of this experiment are the size, shape, rotation and gas production rate.

Size and shape control the volume, the total mass (as a function of bulk density) and therefore the attracting force by the nucleus as a point mass, and perturbing forces defined by the shape and mass inhomogeneities, as expressed by the coefficients of the expanded gravity potential. The available estimates of the nucleus radius from ground and space-based observations show values for Churyumov-Gerasimenko which are definitely larger than those for comet Wirtanen, a fortuitous advantage for this experiment. Ground-based and HST observations have estimated the nucleus radius to be of the order of 2000 m (Lamy *et al*., 2003; Tancredi *et al*., 2000; Kamoun *et al*., 1992). Radar observations constrain the nucleus radius to an upper limit of 3200 m (Kamoun *et al*., 1998). This means that Churyumov-Gerasimenko is at least four times larger than Wirtanen and the point mass attracting force is 50 times stronger for the same bulk density and cometocentric distance. Assuming a radius of 2000 m, the respective point mass is GM = 450–2200 m^3/s^2

for bulk densities between 200 and 1000 kg/m^3. The point mass defines the spacecraft orbit velocity at a given distance, which is of the order of 30 to 66 cm/s for a 5 km orbit distance. The orbital period is correspondingly of the order of one-half to one day.

The estimated rotation period is about 12 hours. At an orbital distance of 5 km, the comet would thus rotate faster below the spacecraft than the spacecraft revolves about the nucleus (neglecting for the moment perturbing forces from comet outgassing, which will prevent the spacecraft from fulfilling a complete and true Kepler orbit).

Only a few observations of the CO gas production rate at heliocentric distances beyond 3 AU are available. This parameter is very important in order to assess the perturbing forces from outgassing when the gravity experiment is performed. An upper limit for the CO production rate of 10^{27} molecules/s was observed by Bocklee-Morvan *et al.* (2004), but models constructed to reproduce these observations yielded production rates one to two orders of magnitudes lower (De Sanctis *et al.*, 2005). A high dust production at large heliocentric distances is made responsible for an even higher CO production rate of 5×10^{27} molecules/s (Fulle *et al.*, 2004), but is thus far not supported by observations of CO (De Sanctis *et al.*, 2005). A water production rate of 10^{28} molecules/s at perihelion is reported by Schulz *et al.* (2004) with an asymmetry around perihelion.

3. Comet Science from Spacecraft Doppler and Range

The scientific objectives of the gravity field investigations are the determination of the mass and bulk density of the nucleus, the low degree and order harmonic coefficients of the gravity field, the cometary moments of inertia, and the nongravitational forces acting on the nucleus. The comet nucleus radius of 67 P/Churyumov-Gerasimenko is estimated to be between 2000 m (Lamy *et al.*, 2003) and 3000 m (Mueller, 1992), four to six times larger than P/Wirtanen. The expected gravity attraction is thus 50 times stronger than at Wirtanen at the same assumed distance to the comet and bulk density. This will allow a more precise mass and density determination at low orbits. First estimates for the Wirtanen mission have been published by Pätzold *et al.* (2001).

3.1. Mass and Bulk Density, Gravity Coefficients and Moments of Inertia

Determination of the cometary mass and bulk density is a fundamental objective required to assess the validity and accuracy of various cometary models. Extensive simulation studies for the Near Earth Asteroid Rendezvous (NEAR) mission to asteroid 433 Eros demonstrated that gravity determinations for a small, irregular asteroid requires a gravity field extraction process fundamentally different from

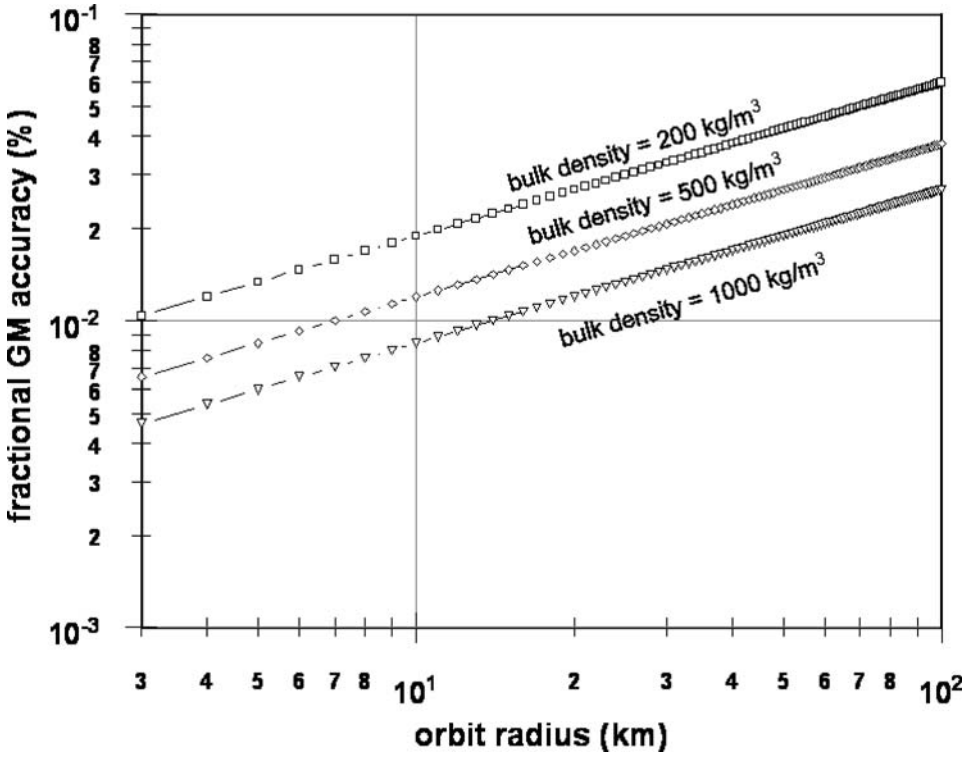

Figure 1. Relative accuracy of the G·M (gravitational constant times body mass) determination as a function of orbital distance of the spacecraft to the nucleus for three different cometary bulk densities. The radius was assumed as 2000 m (Lamy *et al*., 2003).

previous gravity studies of the planets or moons (Scheeres, 1995; Miller *et al*., 1995). By using a combination of optical landmark measurements and Doppler and ranging data, an accurate determination of shape, gravity and rotational state was made for Eros (Miller *et al*., 2002). The coefficients in the gravity field were obtained up to degree and order 10.

Upon arrival at the comet, the nucleus size, shape, mass, activity and spin state will be poorly known. P/Churyumov-Gerasimenko will most likely be active during some portions of the gravity field investigation campaign. A strategy is needed for an iterative solution of the gravity field.

An initial flyby during the Rosetta approach phase should enable a mass determination to an accuracy of 1%. The current size estimate (assuming an albedo between 3 to 4%) of the nucleus radius of 2000 m (Lamy *et al*., 2003) suggests a flyby distance within a few hundred kilometers (Figure 1). Injection into a bound high orbit allows iterative improvements of the mass determination down to a few hundreths of a percent. Retrograde orbits lying in the spin plane of the comet nucleus can have semimajor axes reduced to a few comet radii for the adopted low nominal

rotation period of 67P/C-G, provided that the rotational excitation of the nucleus and the orbital eccentricities are small (Mysen *et al*., 2005).

The second order and degree gravity coefficients (C_{20} and C_{22}) can be estimated using the shape model (from imaging observations) and assuming constant density. The result is a constraint on the true gravity field. In the likely event that the comet is not in perfect principal axis rotation, knowledge of the body's second-order gravity coefficients and a determination of its spin state can be used to determine its moments of inertia; these moments provide constraints upon the internal structure of the nucleus.

The most stable low orbits for the spacecraft will be in equatorial, retrograde orbits about the comet (Mysen and Aksnes, 2005; Mysen *et al*., 2005, Olsen, 2006) or in the terminator plane, provided that the outgassing pressure field is symmetric in this plane (Scheeres *et al*., 1998; Mysen and Aksnes, 2005). Beginning with these orbits, the second-order gravity field can be solved for in the orbit determination process. Higher-order gravity coefficients might be determined from low polar orbits. This strategy also assumes that cometary outgassing does not induce significant accelerations upon the spacecraft. Initial estimates for comet Wirtanen have shown that early activity even beyond 3 AU might generate radial accelerations due to outgassing that could mask the effects of higher gravity harmonics (Gill *et al*., 1996; Pätzold *et al*., 2001). The determination of the higher harmonics would probably only be feasible if a gravity mapping campaign takes place at heliocentric distances well beyond 3 AU when the comet is not very active. In view of the Rosetta mission constraints, a gravity mapping campaign is best performed at heliocentric distances between 3.5 AU and 3 AU (Figure 2) before or at the onset of activity. Unfortunately, the comet will be near solar conjunction at this time, with effects of the interplanetary and coronal medium on the radio wave propagation.

If the gravity mapping campaign must be delayed to times when the comet is already active, care must be taken to ensure that the spacecraft does not become adversely perturbed by the outgassing streams in a direction toward the Sun. If the spacecraft orbit could be maintained nearly perpendicular to the Sun-comet line, the outgassing perturbations would presumably be minimized.

From an improved shape model, the model can be refined and the gravity field can once again be approximated assuming a constant density nucleus. The nucleus mass will eventually be known to 0.001% (Figure 1), volume and density better than 3%. The shape gravity model (with constant density) and the true gravity model (from spacecraft tracking) can then be compared to yield information on the mass heterogeneity of the comet nucleus.

3.2. Nongravitational Forces

The cometary orbit itself is affected by gas and dust emission (a non-gravitational force) during the active phase typically within 3 AU heliocentric distance (Marsden

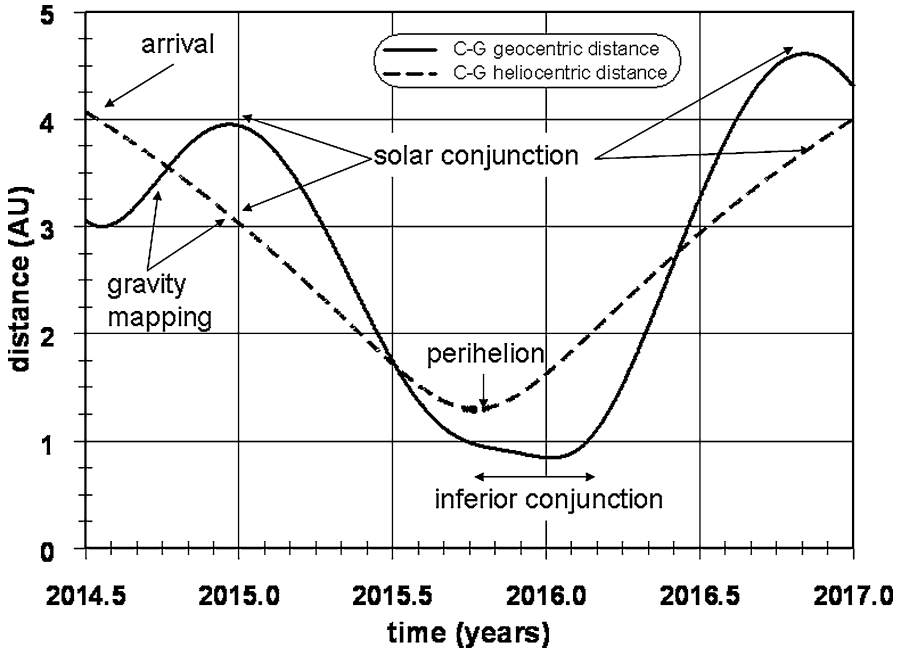

Figure 2. Heliocentric and geocentric distances of comet Churyumov-Gerasimenko during the prime Rosetta mission from July 2014 through December 2017. The optimum time for the gravity mapping campaign is between 3.5 AU and 3.0 AU heliocentric distance before or at the onset of water outgassing activity. Unfortunately, the spacecraft-Earth constellation is approching solar conjunction with extreme effects on the propagation of the radio links. During the perihelion, the constellation is in inferior conjunction.

and Williams, 2005). Recent determinations of the non-gravitational forces acting on 67P/C-G (Krolikowska, 2003; Aksnes and Grav, 2005; Dziak-Jankowska *et al.*, 2005) show that the ougassing from this comet must be relatively weak and repeatable over many apparitions. It was suspected by Boehnhardt *et al.* (1996) that the effects of the nongravitational forces on P/Wirtanen may be very different than previously estimated (Marsden and Williams, 1995) in order to explain the discrepancy between the predicted and observed position of the nucleus at the time of its recovery in 1995. Ground-based astrometry of comets provides only limited spatial accuracy for orbit determination and suffers furthermore, particularly during high activity near perihelion, from the offset between the center of light of the coma and the center of gravity of the nucleus (Yeomans, 1986), the so-called "light shift". The heliocentric position of a spacecraft can be determined very accurately using Doppler and ranging measurements and the relative positions of the spacecraft can be determined using on-board imaging observations. This results in precise observations of the comet's heliocentric position. Along with the comet's existing astrometric data beginning in 1969, it will allow a significant refinement to this comet's nongravitational acceleration force model.

4. Nucleus Investigations: Size and Shape, Internal Structure, Bistatic Radar Experiment

Rosetta is the first spacecraft to use occultation techniques and bistatic radar to explore the properties of a comet's surface and its interior. These radio sounding techniques are well established and have been successfully performed for investigations of planetary rings, atmospheres, ionospheres and surfaces (e.g. Marouf *et al.*, 1982; Tyler, 1987; Tyler *et al.*, 1992). They are currently applied for the investigation of the Martian surface on a routine basis using Mars Express (Simpson *et al.*, 2006) and first observations have been performed at Venus with Venus Express (Häusler *et al.*, 2006).

4.1. Size and Shape, Internal Structure

The size, shape and internal structure of the nucleus are investigated by occultation experiments prior to, during and after the spacecraft is occulted by the nucleus as seen from the Earth. Accurate measurements of the instants of limb ingress and egress determine the length of the occultation chord for a known spacecraft trajectory, hence constraining the size of the nucleus. Repeated measurements for different occultation track geometries constrain the nucleus shape. Occultation observations are most useful when imaging observations are not possible, e.g. for observations of the unlit side or when the limb of the nucleus is obscured by dust.

Because the nucleus is a small body, the interior or the upper layers of the nucleus may be penetrable by microwaves. The refractive properties of the nucleus will modify the propagation of the radio signal enough so that it might be possible to constrain the bulk refractive index of the nucleus.

4.2. Bistatic Radar

A bistatic-radar experiment was proposed to measure the scattering properties of the nucleus, hence determining the physical nature of the surface and its material properties. A bistatic radar experiment is distinguished from a monostatic measurement by the spatial separation of transmitter and receiver (Figure 3). In the Rosetta case the transmitter is the spacecraft, with its High Gain Antenna pointed toward the nucleus surface. The signal is reflected from the surface and received at large ground antennas on Earth.

Monostatic radar observations of comets were conducted with P/Encke (Kamoun *et al.*, 1982), P/Halley (Campbell *et al.*, 1989), IRAS-Aracki-Alcock (Harmon *et al.*, 1989), Hyakutake (Harmon *et al.*, 1997) and P/Grigg-Skjellerup (Kamoun *et al.*, 1999). Rosetta's orbit around the nucleus enables the measurements

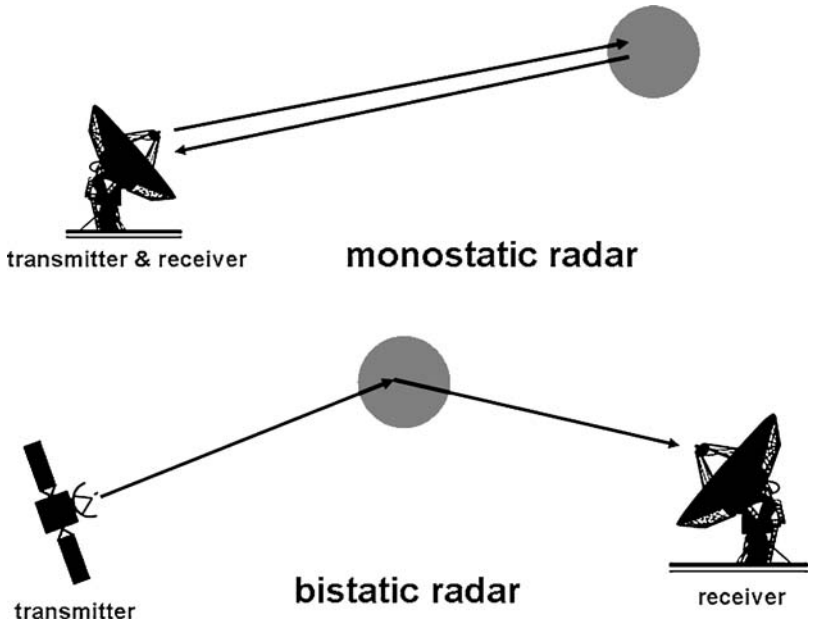

Figure 3. The bistatic radar configuration is distinguished from the monostatic by the spatial separation of transmitter (Rosetta) and receiver (ground station on Earth).

of the strength and state of polarization of the X-band radio signal transmitted by Rosetta and scattered by the nucleus over a broad range of spacecraft-comet-Earth angles. Preliminary link budget studies confirm echo detectability over a broad range of reflection angles for sufficiently close spacecraft orbits within at least 40 km distance to the nucleus. For a nucleus rotating faster than the spacecraft revolves about the nucleus, the reflected echo spectrum will vary considerably about the center frequency (direct signal), thereby allowing a determination of the rotation and precession rates with sufficient accuracy during a single tracking pass. The shape and strength of the co- and cross-polarized components of the echo spectra can be used to differentiate between asteroid-like diffractive surface scattering (Ostro, 1985; Harmon *et al*., 1989) and icy-body-like volume scattering (Ostro *et al*., 1992). Furthermore, for the circularly polarized incident wave, detection of the special bistatic scattering angle at which the co- and cross-polarized components are nearly equal in strength (the echo is roughly linearly polarized) determines the Brewster angle γ_B of the surface material, hence its dielectric constant $\varepsilon = \tan^2 \gamma_B$. In principle, independent differentiation between icy conglomerate ($\gamma_B \sim 50^\circ$, $\varepsilon \sim 1.4$) and very dusty ($\gamma_B \sim 60^\circ$, $\varepsilon \sim 3$) surfaces can thus be achieved. Similar bistatic radar observations were used to determine ε of the lunar crust (Tyler and Howard, 1973) and the Martian surface (Simpson and Tyler, 1981).

5. Coma Investigations

The abundance of mm to dm size dust grains near the nucleus, the plasma content of the very inner coma inaccessible to orbiter *in situ* measurements and the combined dust and gas mass flux perturbing the Rosetta spacecraft orbit are the objectives of the cometary coma investigations.

5.1. Abundance of mm-dm Size Cometary Dust

Radar observations of comets Iras-Araki-Alcock (Harmon *et al*., 1989) and Halley (Campbell *et al*., 1989) revealed a dust grain size population between a few mm and probably as large as 10 cm distributed about the nucleus out to distances of 1000 km. The wavelengths used by the Rosetta radio subsystem are in the same bands used in these radar studies. The dominant contributors to the total mass intercepted during the Giotto flybys at Halley and Grigg-Skjellerup were dust grains of a few mm (Pätzold *et al*., 1991b; 1993). Richter and Keller (1995) studied the influence of the radiation pressure force on the orbital evolution of dust grains up to 10 cm in size around cometary nuclei. They concluded that large grains might survive in stable orbits for an entire orbital revolution of the comet.

One observable of the cometary grain sounding experiment will be the signal attenuation along the ray path from the spacecraft to the Earth, expressed as the optical depth $\tau(\lambda)$. The value for X-band, $\tau(3.6\,\text{cm})$, reflects the contribution for all grains larger than a few mm and the differential optical depth, $\tau(3.6\,\text{cm}) - \tau(13\,\text{cm})$, constrains the contribution to grains in the mm – dm size range (Marouf *et al*., 1982). The second observable is the power incoherently scattered in the near-forward direction. Because of the motion of the grains relative to Rosetta and the Earth, the scattered signal is Doppler shifted and spread over a finite bandwidth centered on the frequency of the direct ray. The detectability of these observables strongly depends on the abundance and size distribution of the mm and larger size particles. A search by Rosetta for attenuation and near-forward scattering effects during coma occultation events will either determine or set limits on the abundance of such particle sizes using techniques similar to those used to study planetary rings (Marouf *et al*., 1983; Tyler *et al*., 1983).

5.2. Plasma Content

The first radio sounding observations of a cometary ionosphere were performed with the VEGA spacecraft at comet P/Halley. They revealed the mean large-scale electron density distribution and were able to resolve the inner "pile-up" region (Andreev and Gavrik, 1990; Pätzold *et al*., 1997). Observations at two coherently related frequencies are required to separate the dispersive contribution from the classical Doppler shift.

With Rosetta it is possible to access in particular those coma and jet regions which will not be investigated *in situ*. Preliminary estimates indicate that a differential phase shift is detectable for gas production rates between 10^{27} to 10^{28} molecules/s (v. Oertzen, 2003).

5.3. Combined Gas and Dust Mass Flux

The motion of the Rosetta spacecraft about the nucleus is perturbed by mostly radial accelerations due to gas and dust impinging on its surface. These orbit perturbations are detectable from Doppler shifts of the radio signal to Earth. It may thus be possible to determine the combined gas and dust mass flux and its variation with distance from the nucleus, its evolution with heliocentric distance and the variation of coma and jet activity with solar illumination. The entire cross-sectional area of the spacecraft (the solar cell array alone measures about 64 m^2) serves as a detector for the impinging coma material. The impact of individual large dust grains (larger than 1 mm in diameter) may be detectable. In contrast to the Giotto flybys (Pätzold *et al*., 1991a), however, the main perturbations are expected to be due to gas jets rather than dust grain impacts. Together with the gravity field modeling, RSI is able to constrain the maximum liftable mass and can also provide an estimate of the overall gas and dust production rate.

6. Asteroid Flybys

A spacecraft's velocity is perturbed by the attracting forces of asteroids or other bodies during sufficiently close flybys. The spacecraft is accelerated toward the asteroid along its flyby trajectory. The analysis of the resultant velocity changes ultimately yields a measure of its total mass or GM (gravitational constant times mass). The bulk density is determined from the mass determination and the volume estimate made by the imaging system. Mass and bulk density estimates of asteroids have thus far only be obtained from the Galileo flyby at the asteroid Ida and from the NEAR flybys at the asteroids Mathilde and Eros. Asteroid Ida was too small to perturb the flyby trajectory of Galileo above the treshold of detectability. The discovery of Ida's moon Dactyl, however, provided an unexpected opportunity to estimate Ida's mass and bulk density. Mathilde's bulk density was found to be surprisingly low.

After a successful launch and a highly precise orbit injection and trajectory maneuver, it was possible to select two potential target asteroids which fulfill the Δv constraints within the available fuel. The selected asteroids are Lutetia at a size of 100 km, comparable with Siwa from the old Wirtanen mission, and Steins at a size of about 10 km (Table I). Lutetia would probably be massive enough to achieve a mass density determination as estimated for the Siwa flyby (Pätzold *et al*., 2001b).

TABLE I
Asteroid flyby parameters.

	Steins	Lutetia
Flyby date	5 September 2008	10 July 2010
Time of closest approach (UTC)	18:30:26	15:54:30
Size	17.5–5.5 km[a]; <4.6 km[b]	95.8 ± 4.1 km[c]
Density	2000 ± 500 kg/m^3	2000 ± 500 kg/m^3[d]
Asteroid class	E[c]	C (or M)[c+e]
Flyby velocity	9.0 km/s	15.0 km/s
Minimal flyby distance	600 km	1600 km
Nominal flyby distance	1760 km	3004 km
Angle between relative flyby velocity vector and direction to earth	81°	113°
Distance Earth-Rosetta	2.4 AU	3.0 AU
Closest Distance between signal and sun	192 R_{SUN}	193 R_{SUN}
Sun-Earth-Rosetta angle	62°	62°

[a]Depending on albedo values of 0.04–0.4, Barucci *et al*. (2005).
[b]Fornasier *et al*. (2006).
[c]Barucci *et al*. (2005).
[d]Lazzarin *et al*. (2004).
[e]Estimated range.

The ability to determine the mass and bulk density of the asteroid depends crucially on the flyby distance and relative flyby speed. Figure 4 shows a simulated flyby for the interval ±1.5 h about closest approach to the asteroid Lutetia. The final Δv of the curves shown for different bulk densities is essentially a measure of GM and therefore the mass of the body (Pätzold *et al*., 2001a):

$$\Delta v(\infty) = -2\frac{\mathrm{GM}}{d \cdot v_0}\sin\alpha \tag{1}$$

where d is the closest approach distance to the asteroid and v_0 is the relative flyby velocity and α is the angle between the flyby trajectory and the line-of-sight between the spacecraft and Earth.

A change in velocity can be resolved for flyby distances within 10,000 km at Lutetia because of its relatively large size. The accuracy of the GM determination (Anderson *et al*., 1992)

$$\frac{\sigma_{\mathrm{GM}}}{\mathrm{GM}} = \frac{d \cdot v_0}{\mathrm{GM}}\sigma_v \tag{1.1}$$

is estimated to be fractions of a percent at a distance of 3000 km with an expected velocity noise of 350 μm/s. RSI encounter operations will begin about five hours before closest approach for a total tracking time during the encounter period of 10 h. Two further 10 h tracking passes, one after the last spacecraft maneuver

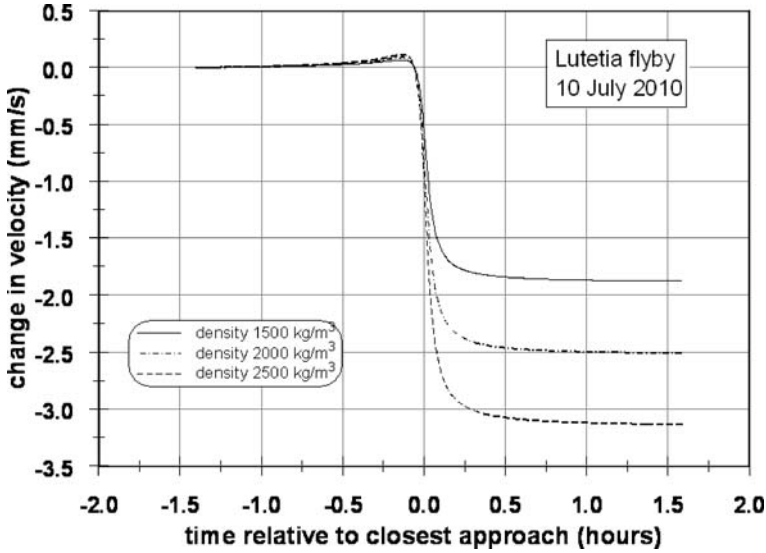

Figure 4. Predicted changes in spacecraft velocity as a function of time relative to the closest approach to asteroid Lutetia for a closest approach distances at 3,000 km and for three different bulk density models. The size of the asteroid was assumed as 100 km. The final Δv of 2–3 mm/s is ultimately a measure of G·M. The expected noise at 600 s integration is 10 μm/s.

before closest approach and one before the first spacecraft maneuver after closest approach and both within 48 h centered about closest approach, will be used for the establishment of a pre- and post-encounter baseline.

The second asteroid, Steins, is probably much smaller than Otawara from the old Wirtanen mission (Fornasier *et al*., 2006). Although the current baseline calls for a flyby at about 1760 km distance, a 600 km flyby distance seems to be feasible but would in any case yield an undetectable change in velocity.

7. Radio Sounding of the Solar Corona

The Rosetta spacecraft will undergo superior solar conjunction six times during the cruise, providing opportunites for radio sounding of the inner solar corona. Furthermore, two solar conjunctions occur during the prime mission at the comet.

The constellation of superior solar conjunction occurs when the spacecraft is behind the Sun as seen from the Earth. Radio Science defines a solar conjunction phase when the spacecraft is within 10° elongation from the solar disk in the plane of sky. Radio signals transmitted from Earth to the spacecraft and back must propagate through the dense plasma of the solar corona. The propagation medium induces phase shifts onto the carrier frequencies and time delays onto the ranging

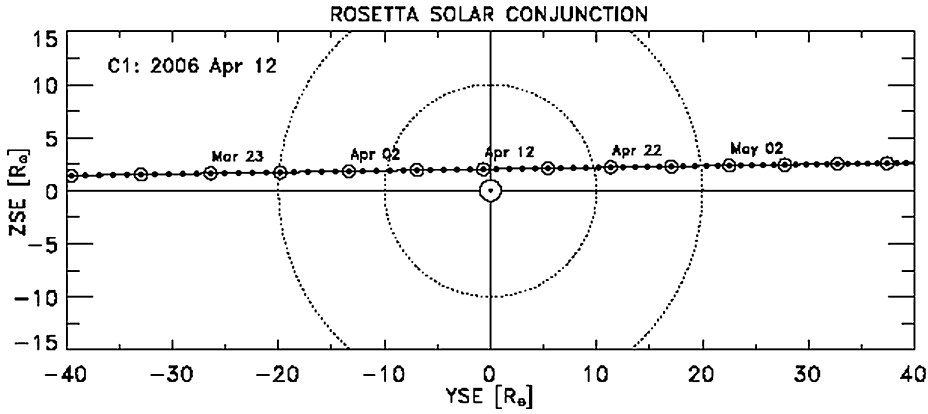

Figure 5. Rosetta superior solar conjunction geometry in the plane-of-sky in 2006. Each dot marks the daily position of Rosetta in the plane-of-sky within 40 solar radii (10° elongation) relative to the solar disk.

signals which can be used to determine the absolute coronal electron content and its variations, the large-scale structure, the solar wind speed in its acceleration regions, and potentially reveal the cross-sectional morphology of coronal mass ejections (CME).

Preparations have been made for operations during the first solar conjunction of this mission in April 2006, when the spacecraft offset from the Sun is within ±40 solar radii (10° elongation). As seen from the Earth (Figure 5), the spacecraft appears to pass over the northern pole of the Sun. Forty-three tracking passes, with an average of four hours each, are scheduled at the ESA ground station in New Norcia. Another solar conjunction will occur at the end of 2008, followed by four others in the fourth quarters of 2010, 2011, 2012 and 2013.

Rosetta and its target comet will approach solar conjunction near their initial encounter. This circumstance will not be favorable for RSI cometary radio science observations between 3.5 and 3.0 AU heliocentric distance.

8. Technical Description

8.1. Rosetta Radio Subsystem

Rosetta is capable of receiving and transmitting radio signals via any of three antenna systems (Figure 6):

- High Gain Antenna (HGA): steerable parabolic dish, diameter: 2.20 m, gain:, 40 dBi (X-band), 28 dBi (S-band)
- two medium gain antennas (MGA)
- two Low Gain Antennas (LGA), front and rear side

Figure 6. The antenna systems of the Rosetta spacecraft: the High Gain Antenna (HGA) is a parabolic dish of 2.20 m diameter and used as the primary antenna for RSI. Furthermore there are two Medium gain Antennas (MGA) side by side for separate X-band and S-band transmissions and two Low Gain Antennas (LGA, one at the rear and one at the front) for near Earth communications and emergencies.

A block diagram of the characteristic features of the Rosetta radio subsystem is shown in Figure 7. Each of the two redundant transponders is comprised of receivers and transmitters at both S-band and X-band. The X-band transmitter output is amplified by one of two redundant 20 W Travelling Wave Tube Amplifiers (TWTAs), the S-band downlink by a Solid State Amplifier of 5 W RF output. The spacecraft is capable of receiving and transmitting at S-band (2.1 GHz) via the LGAs, or receiving at either X-band (7.1 GHz) or S-band via the HGA. The right-handed circular polarized (RCP) downlink signals at S-band (2.3 GHz) and X-band (8.4 GHz) are transmitted via the HGA simultaneously (see an overview of frequencies in Tables II and III). The HGA (Figure 6) is the primary antenna for receiving telecommands and transmitting high rate telemetry in the operational phase. The LGAs are used during the commissioning phase and emergency operations.

TABLE II

X-band one sigma r.m.s. values and Allan deviation from the USO checkouts.

					Allan deviation ($*10^{-13}$)		
Date	DOY	Distance to earth (AU)	r.m.s frequency (mHz)	r.m.s velocity (10^{-6} m/s)	Int.-time 1 s	Int.-time 10 s	Int.-time 100 s
29.03.2004	089	0.06	2.264	81	2.41	0.96	0.89
02.05.2004	133	0.17	2.421	86	2.47	1.28	0.49
10.10.2004	283	0.45	2.984	107	3.06	1.31	0.55
06.04.2005	096	0.07	3.93	140	5.2	1.4	0.4
29.09.2005	272	1.42	3.582	128	4.88	0.96	0.27
02.03.2006	061	2.62	7.000	250	8.52	2.47	1.44
22.08.2006	234	2.03	8.433	301	7.73	4.22	4.35

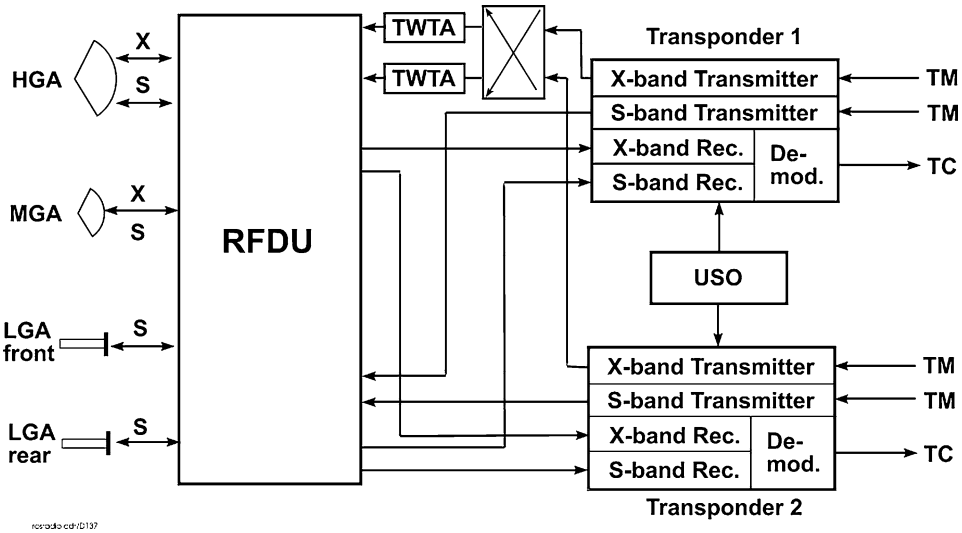

Figure 7. Principal block diagram of the Rosetta radio subsystem. The Ultrastable Oscillator (USO) serves as a frequency reference source for the one-way downlink. The X-band signals are amplified by Traveling Wave Tube Amplifiers (TWTA). The Radio Frequency Distribution Unit (RDFU) connects the antennas with the input and output signals of the two transponders.

RSI uses two radio link modes (Figure 8):

- The coherent two-way radio link is established by transmitting an X-band uplink radio signal to the spacecraft. The uplink signal frequency is multiplied in the transponder by 880/749 and 240/749 to generate downlink signals at X-band and S-band, respectively. The ratio of both frequencies is $880/240 = 11/3$. The

TABLE III
Two-way X-band r.m.s. and Allan deviation values.

					Allan deviation ($*10^{-13}$)		
Date	DOY	Distance to earth (AU)	r.m.s frequency (mHz)	r.m.s velocity (10^{-6} m/s)	Int.-time 1 s	Int.-time 10 s	Int.-time 100 s
29.03.2004	089	0.06	3.29	117	3.44	1.77	0.68
02.05.2004	133	0.17	2.24	90	3.11	0.5	0.25
10.10.2004	283	0.45	5.58	199	4.38	4.01	1.08
06.04.2005	096	0.07	2.44	87	3.26	0.86	0.2
29.09.2005	272	1.42	5.99	214	7.78	2.04	1.16

two-way radio mode takes advantage of the superior frequency stability inherent to the hydrogen maser oscillator at the ground station on Earth. This mode is used for sounding the cometary atmosphere and ionosphere, the gravity science applications, and sounding the solar corona.

- The one-way link mode is established by transmitting simultaneously and phase coherently the X-band and S-band downlinks, stabilized by the onboard Ultra-stable Oscillator (USO) which is connected to both transponders but drives only one set of X- and S-band transmitters in one transponder.

8.2. Ground Segment

Ground stations (Figure 9) include antennas, associated equipment and operating systems in the tracking complexes of New Norcia (ESA, 35 m), Australia, and the Deep Space Network, DSN (NASA, 34 m and 70 m) in California, Spain, and Australia. A tracking pass consists of typically eight to ten hours of spacecraft visibility and communication at the respective ground station site. Measurements of the spacecraft range and carrier Doppler shift can be obtained whenever the spacecraft is visible and its HGA is pointed toward the Earth.

In the two-way mode the ground station transmits an uplink radio signal at X-band and receives the dual-frequency downlink at X-band and S-band. Information about signal amplitude, received frequency and polarization is extracted and stored as a function of ground receive time.

ESA's 35 m ground station (Figure 9) at New Norcia (NNO), Australia, is located about 200 km north of its present tracking complex in Perth. The station equipment consists of three identical new receiving systems designated as the Intermediate Frequency and Modem System (IFMS). One of these is dedicated to radio science closed-loop and open-loop data recording of the Mars Express and Venus Express

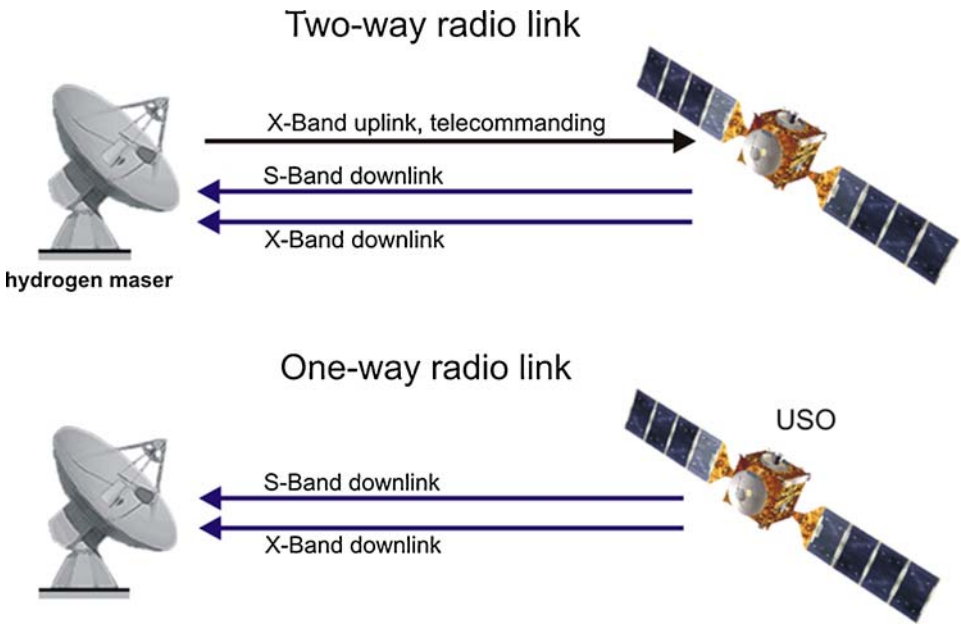

Figure 8. RSI radio link modes.

radio science investigations (Pätzold *et al.*, 2004, 2006; Häusler *et al.*, 2006) and the Rosetta Radio Science Investigations (RSI) experiment. The open-loop system will be used specifically for the radio sounding of the atmosphere/ionosphere, bistatic radar and solar corona investigations where closed-loop tracking receivers would typically lose lock. The IFMS operates on a 17.5 Msps 24-bit complex baseband stream (containing 12 bit words each for the I and Q channels) generated from filtering and decimating the 280 Msps 8-bit stream output data from the Common Front End Analogue to Digital converter. These channels are provided for both RCP and LCP polarizations. The Radio Science raw data can be directly transferred to a mass storage device and/or processed by a Fast Fourier routine.

In principle, radio science measurements in the ground stations can be done simultaneously on a noninterference basis with the transmission of telemetry and/or reception of telecommands. However, since the signal-to-noise ratio of the carrier signal is considerably reduced when transmitting telemetry, an unmodulated downlink radio carrier is preferred for most applications.

8.3. Observed Quantities

The data from both receiver systems, closed-loop and open-loop, can be generated simultaneously regardless of the radio link configuration, one-way or two-way. The received carrier frequencies, the signal strengths (received total power) and the

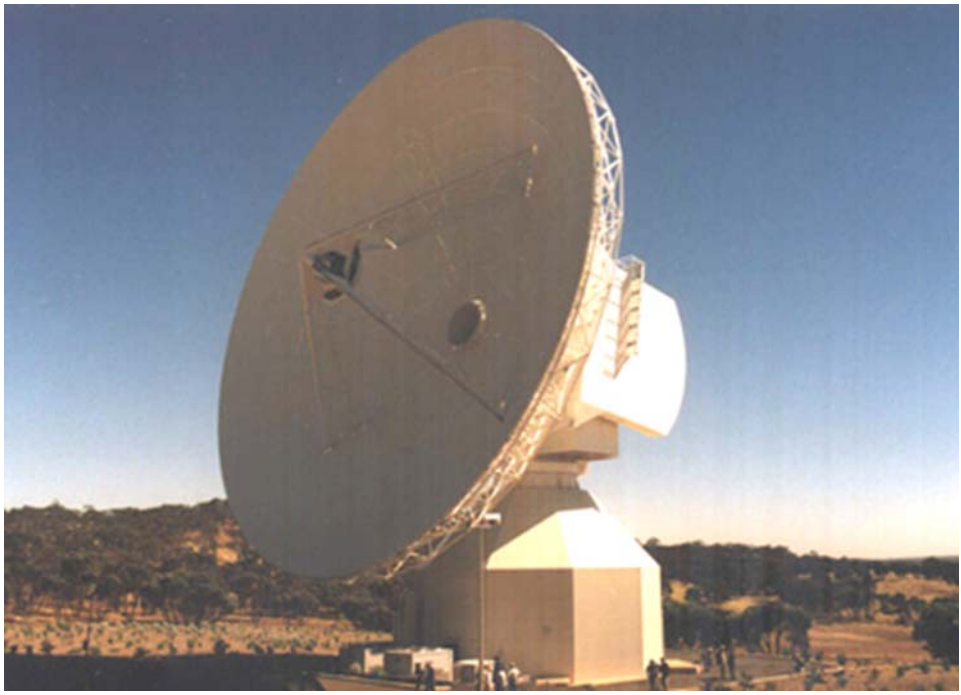

Figure 9. ESA's 35-m deep space antenna in New Norcia, West-Australia serves as the primary receiving antenna for the mission and for RSI. Three IFMS receiving systems, one dedicated for RSI observations, provide X-band uplink signals and reception and recording of Doppler, range, polarization at X-band and S-band.

polarization of the radio signals are monitored at the ground station. Radio metric data are recorded by the so-called closed-loop receiver system:

- Doppler frequency shifts (one-way and two-way mode)
- Received signal power (AGC)
- Ranging measurements (two-way mode only)
- Meteo data from the ground station site

8.3.1. *Doppler Shift*

The transmission of dual-frequency phase-coherent downlinks at S-band and X-band with the constant ratio 11/3 makes it feasible to separate the dispersive from the nondispersive Doppler effects on the radio link.

The frequency of the radio carrier is shifted according to the relative radial velocity between the transmitter and the receiver (classical Doppler shift). Furthermore, a relative phase shift is experienced when the radio wave propagates through an ionized medium (ionospheres, interplanetary medium, solar corona). Excluding

oscillator drifts and instabilities, the frequency shift for a one-way (spacecraft-to-Earth) radio link due to plasma is

$$\Delta f = f - f_0 = -\frac{f_0}{c}\frac{ds}{dt} + \frac{40.31}{c}\frac{1}{f_0}\frac{d}{dt}\int_{s/c}^{\text{Earth}} N_e(s)\,ds \tag{2}$$

where ds/dt is the rate of change of the distance between transmitter and receiver (relative velocity), c is the speed of light and f_0 is the carrier frequency. The integral of the electron density N_e(s) along the propagation path ds of the radio wave from the spacecraft (s/c) to Earth is called the columnar electron content, or column density.

The first term on the right hand side of (2) is the classical Doppler shift (linear in f_0 in first order) and the second term is the dispersive propagation effect of radio waves in ionized media which is inversely proportional to f_0. A larger classical Doppler shift is measured on the X-band, but the lower S-band frequency is more sensitive to dispersive frequency shifts. A change in relative velocity of 2 cm/s yields a classical Doppler frequency shift of 0.6 Hz at X-band. A dispersive frequency shift of 0.6 Hz at S-band is produced by a change in electron content by one hexem (10^{16} electrons/m^2) within one second.

It is not possible to separate classical and dispersive frequency shifts from the observed total change in frequency Δf at either f_S or f_X, the S-band or X-band carrier frequency, respectively, alone. However, using (2) for the two phase-coherent downlinks at X-band and S-band with a constant transponder ratio of $880/240 = 11/3$ and calculating the differential Doppler $\Delta f_S - \frac{3}{11}\Delta f_X$ where Δf_S and Δf_X are the observed Doppler shifts at S-band and X-band, respectively, it is possible to isolate the dispersive frequency shift:

$$\begin{aligned}\Delta f_S - \tfrac{3}{11}\Delta f_X &= -\frac{\frac{d}{dt}s}{c} f_S + \frac{40.31}{c}\frac{1}{f_S}\frac{d}{dt}\int_{s/c}^{\text{Earth}} N_e ds + \tfrac{3}{11}\frac{\frac{d}{dt}s}{c} f_X \\ &\quad - \tfrac{3}{11}\frac{40.31}{c}\frac{1}{f_X}\frac{d}{dt}\int_{s/c}^{\text{Earth}} N_e ds \\ &= \frac{40.31}{c} f_S\left[\frac{1}{f_S^2} - \frac{1}{f_X^2}\right]\frac{d}{dt}\int_{s/c}^{\text{Earth}} N_e ds \end{aligned} \tag{3}$$

The "differential Doppler effect" (3) calculated from the observed frequency shifts is proportional to the change in electron content. All oscillator drifts and relative velocities are eliminated in this process. The result can further be used to correct each single classical frequency shift for the dispersive propagation effects.

The example above was derived for a one-way link. It can be shown that the calculation of the differential Doppler of a two-way radio link, when the spacecraft transmitted carrier frequencies are derived coherently from the received (and Doppler shifted) uplink frequency, leads to exactly the same relation (3). Integration of (3) with respect to time yields the differential phase, which is proportional to

changes in electron content along the downlink from the beginning of the tracking pass.

8.3.2. *Ranging (Propagation Delay)*
The *absolute value* of total electron content can be determined from the differential propagation delay by two-way ranging at S-band and X-band:

$$\tau_S - \tau_X = \frac{40.31}{c}\left\{\frac{1}{f_S^2} - \frac{1}{f_X^2}\right\}\int_{s/c}^{\text{Earth}} N_e\, ds \tag{4}$$

Typically, the Doppler or phase measurements are more sensitive than the ranging measurements by about two orders of magnitude.

9. First Observations During Cruise

The stability of the radio links used for the various RSI experiments defines the accuracy of the observations and is therefore of essential importance for RSI. The data quality of the one-way radio link is determined mainly by the behaviour of the Ultrastable Oscillator (USO), the performance of the onboard transponder and the receiver equipment in the ground station. The stability is measured in terms of the Allan deviation $\Delta f/f_0$ where Δf is the frequency noise and f_0 is the carrier frequency. The requirement for the Rosetta USO was specified as $\frac{\Delta f}{f_0} \leq 10^{-13}$ for integration times between 3 seconds and 100 s. The USO must be checked regularly during the mission in order to monitor the Allan deviation as a function of geocentric distance as well as the ageing and drift of the quartz oscillator.

The two-way radio link stability is governed by the ground station hydrogen maser (Allan deviation $\approx 10^{-15}$ at 100 s integration time) and typically superior to the USO stability at the same integration time.

The one-way radio link driven by the USO was compared to the coherent two-way radio link with X-band uplink during the Near Earth Verification Phase. The first tests in March 2004 were followed by further tests in May and October 2004. Additional data could be obtained during the first four Passive Checkouts (PC0 to PC3) in 2005 and 2006 (see Table II).

Figure 10 shows a typical timeline of one-way USO frequency residuals recorded during the Passive Checkout 1 (PC1) on 29 September 2005 at a geocentric distance of 1.42 AU. The frequency residuals are the difference, the observed minus the predicted carrier frequency, where the latter quantity was computed from knowledge of the actual interplanetary orbit and accounting for perturbations from all known gravitational and nongravitational forces acting on the spacecraft. Frequency residuals reveal other perturbing forces or frequency shifts due to media propagation effects which have not been considered tn the prediction. For this case, a spacecraft in interplanetary cruise, the frequency residuals reveal the total system noise and

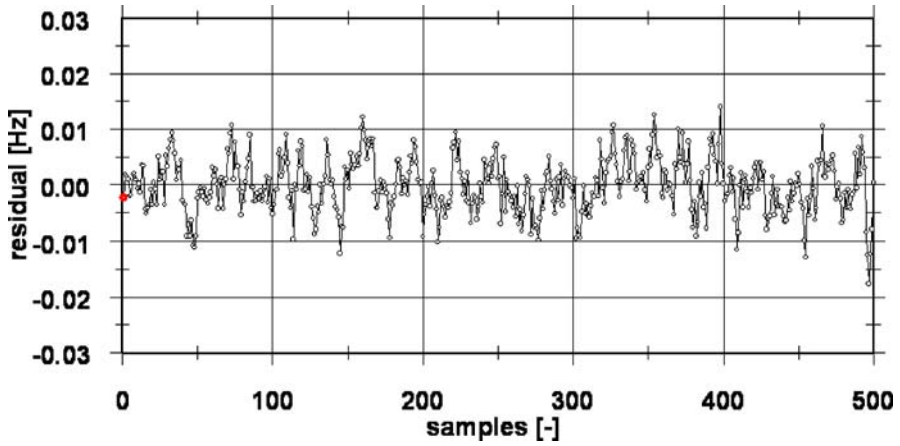

Figure 10. USO one-way X-band frequency residuals (observed minus predicted frequency) at a sample rate of one sample/second. The recording was made on 29 September 2005 at a geocentric distance of 1.42 AU. The one sigma noise is 3.6 mHz or correspondingly 128 μm/s.

thus provide an assessment of the accuracy expected for future observations. The standard deviation of the measurements in Figure 10 is 3.6 mHz at X-band, which translates to a mean Doppler deviation of $\sigma_{v0} = 171$ μm/s at one second integration time. For longer integrations, the accuracy $\sigma_v(\Delta t)$ scales with the square root of the integration time Δt:

$$\sigma_V(\Delta t) = \sigma_{V0}\frac{1}{\sqrt{\Delta t}} \tag{5}$$

In view of the very small orbital velocities and revolution periods about the nucleus, typical integration times used in the gravity science investigations are in the range between 60 s and 600 s for the asteroid flybys and for the determination of the nucleus mass.

Table II summerizes the X-band noise studies from the various USO tests already performed with Rosetta. The USO will be checked every six months during the Passive Checkouts as well as during the Active Checkouts.

The Allan deviation of the USO was specified as 10^{-13} for integration times of less than 100 s at X-band. Table II shows that this order of magnitude was achieved even at large geocentric distances. The value for 6 April 2005 (DOY 096) was computed from the tracking pass on the MGA during the Earth flyby.

In comparison with the USO data, Figure 11 shows a time series of two-way X-band data recorded on the same day, 29 September 2005. The one sigma r.m.s. is 5.99 mHz or 214 μm/s.

Figure 12 shows computed theoretical radio link budgets for Rosetta at X-band for geocentric distances between 0.1 and 3.6 AU. The calculations assume RF transmitted power of 20 Watt, a spacecraft HGA gain of 43 dBi, a 35-m ground

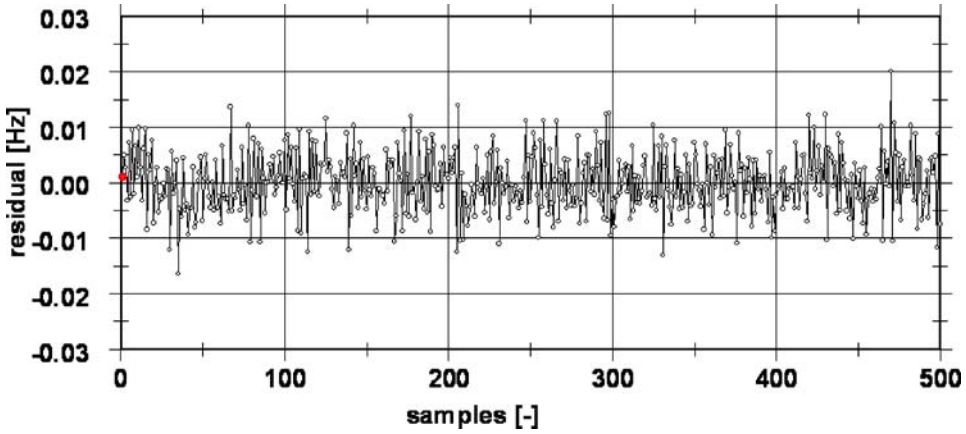

Figure 11. Two-way X-band frequency residuals at a sample rate of one sample/second from the 29 September 2005 recordings at a geocentric distance of 1.42 AU. The one sigma noise is 6 mHz or 214 μm/s due to the accumulation of noise on the uplink and downlink.

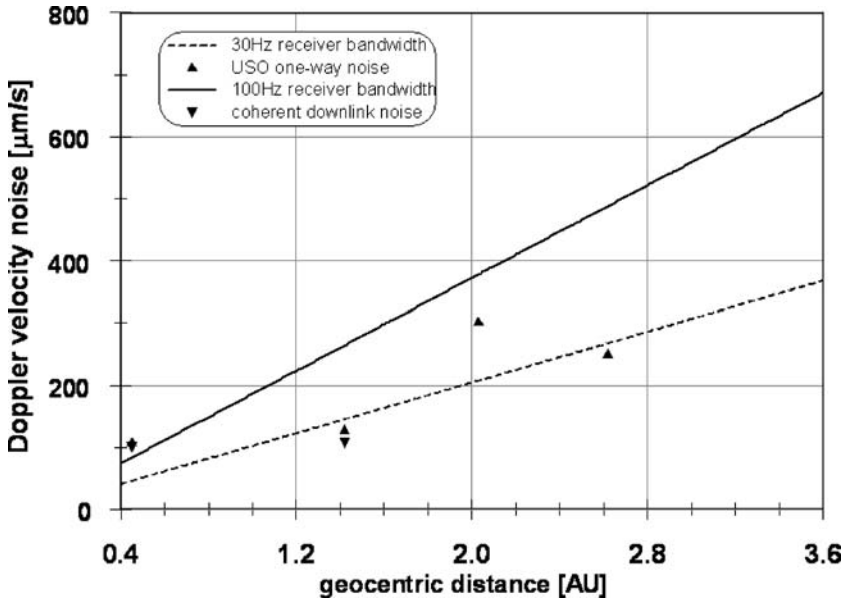

Figure 12. Estimated 1-sigma Doppler velocity noise for two ground station receiver bandwidths at 30 Hz and 100 Hz. The triangles mark the observed USO one-way and the coherent downlink Doppler velocity noise from the two-way link if available. Extrapolating the Doppler noise to 3.5 AU yields 350 μm/s for a 30 Hz bandwidth corresponding to 3×10^{-8} m/s^2 acceleration noise.

station gain of 79.4 dBi with an associated noise level of 180 dBm/Hz for different bandwidth B, and a one second integration time. The one-way USO noise levels and the downlink two-way noise levels translated into downlink noise values are marked by symbols which coincide very well with expected theoretical values.

TABLE IV

Forces (expressed as acceleration) acting on the spacecraft near the comet.

	Value (m/s^2)	Comment
Expected acceleration noise level at X-band	3×10^{-8}	At 3.5 AU, bandwidth 30 Hz, integration time 600 s
Nucleus gravity field:		
GM	4×10^{-5}	Point mass at 5 km distance
C_{20}	10^{-6}	Amplitude at 5 km distance
Solar radiation pressure on full solar cell area of 70 m^2	10^{-9}	At 3 AU heliocentric distance
	10^{-8}	At 1.3 AU Heliocentric distance
Mass flux:		
Gas production rate 10^{23} s^{-1}	10^{-10}	S/C Cross sectional area 10 m^2
Gas production rate 10^{25} s^{-1}	10^{-8}	S/C Mass 1800 kg
Gas production rate 10^{26} s^{-1}	10^{-7}	At 5 km Distance
Gas production rate 10^{28} s^{-1}	10^{-5}	
Dust production rate 200 kg/s	10^{-8}	

Extrapolating these theoretical noise values to larger geocentric distances would define the approximate expected noise levels for operations at the comet. Assuming a receiver bandwidth of $B = 30$ Hz, the expected noise level would be 350 μm/s at one second integration time, and about 20 μm/s at 600 s integration time. The latter value corresponds to an acceleration noise level of $\sigma_a = 3 \times 10^{-8}$ m/s^2. Further reduction of the receiver bandwidth, if practicable, may reduce this value and scales as $\sigma_{a,B_1} = \sigma_{a,B_2}\sqrt{\frac{B_1}{B_2}}$.

Table IV shows a comparison of some forces (expressed as an acceleration) acting on the spacecraft when at the comet: nucleus gravity field, solar radiation pressure, outgassing mass flux as a function of water production rate, dust mass flux. The strength of the radiation pressure depends on the heliocentric distance, while the mass flux pressure depends on comet activity (and therefore also on heliocentric distance), distance to the comet and exposed cross- sectional spacecraft area, which may vary between 6 m^2 (edge on to the mass flow $\rightarrow$ best case) and 70 m^2 (includes fully exposed solar cell array $\rightarrow$ definitely worst case for controlling the spacecraft in stable orbits).

The attracting force by the nucleus gravity field depends on cometocentric distance (for a given mass and shape). The radial mass flux pressure from the outgassing (depending on cometary activity, s/c cross sectional area and distance) counteracts the attracting force and may eventually overcome and "blow" the spacecraft away from the highly active comet close to perihelion. It is thus necessary to determine the nucleus gravity field before the onset of activity or when the nucleus is not

very active within 3.5 AU heliocentric distance. Otherwise, even small gas production rates may mask the contributions from the low degree and order gravity harmonics. It is expected that the low order degree and order gravity coefficients may be extracted within ten kilometers distance if the gas production rate is below $10^{26}\,s^{-1}$.

10. Summary

The first measurements and check-outs during cruise have shown that the Rosetta subsystem configuration is capable to fulfill the experiment goals. Table IV lists the potentially achievable sensitivities for the various experiments. The precise determination of the nucleus and bulk density and potentially the low degree and order gravity field will lead to refined models of the nucleus interior. The study of the perturbing forces by outgassing along the spacecraft orbit will reveil gas and dust production rates and their variations. A bistatic radar experiment will study the overall roughness and composition of the nucleus surface. However, after arrival at the comet and shortly before the start of science operations, the comet will pass into the phase of superior solar conjunction as seen from the Earth which will lead to radio signal degradation and increased noise. The determination of the cometary gravity field will become a challenge in this situation when performed between 3.5 AU and 3.0 AU heliocentric distance. It cannot be delayed because of the increasing cometary activity which will induce further perturbing forces on the spacecraft masking the influence from the gravity field.

Rosetta is still eight years away from arrival at the comet. Detailed planning of science operations can only be done based on a profound knowledge of the cometary physical parameters and activity. The estimates in this work have been based on the observations of 67 P/Churyumov-Gerasimenko reported by Lamy *et al*. (2003). Recent ground based observations of P/Churyumov-Gerasimenko at aphelion and opposition have shown that the size of the nucleus may even be larger (Lowry *et al*., 2006).

Acknowledgements

It is a pleasure to thank all Rosetta project personnel at ESTEC, ESOC and Astrium for their efforts to make the Rosetta mission a success. In particular, we want to thank the participants of the RSI Progress Meetings for their cooperation and understanding of the special requirements of a radio science experiment: C. Berner (ESTEC), B. Gramkow (ESTEC), R. Heinze (Astrium), G. Schwehm (ESTEC), M. Sweeney (ESOC). The Rosetta RSI experiment is/was funded and supported by Deutsches Zentrum für Luft- und Raumfahrt (DLR) Bonn, Germany, under grants 50QP9713 and 50QP0405; Ministerium für Schule und Weiterbildung, Wissenschaft und Forschung des Landes Nordrhein-Westfalen, Düsseldorf, Germany;

Universität der Bundeswehr München, Neubiberg, Germany; the Centre Nationale d'Etude Spatiale (CNES), Paris, France; University of Oslo, Oslo, Norway, and the National Aeronautics and Space Administration (NASA), Washington DC, USA.

References

Aksnes, K., and Grav, T.: 2005, *Astron. Astrophys.* **441**, 815.

Anderson, J. D., Krisher, T., and Borutzki, S., *et al.*: 1987, *Astrophys. J.* **323**, L141.

Anderson, J. D., Armstrong, J. W., Campbell, J. K., Estabrook, F. B., Krisher, T. P., and Lau, E. L.: 1992, *Space Sci. Rev.* **60**, 591.

Anderson, J. D., Lau, E. L., Sjogren, W. L., Schubert, G., and Moore, W. B.: 1997, *Science* **176**, 1236.

Anderson, J. D., Schubert, G., Jacobson, R. A., Lau, E. L., Moore, W. B., and Palguta, J. L.: 2004, *Science* **305**, 989.

Andreev, V. I., and Gavrik, A. L.: 1990, *Kosmicheskie Issledovaniya* **28**, 293.

Barucci, M. A., Fulchignoni, M., Fornasier, S., Dotto, E., Vernazza, P., Birlan, M., *et al.*: 2005, *Astron. Astrophys.* **430**, 313.

Bird, M. K., Volland, H., Pätzold, M., Edenhofer, P., Asmar, S. W., and Brenkle, J. P.: 1994, *Astrophys. J.* 426, 373.

Bird, M. K., Allison, M., Asmar, S. W., Atkinson, D. H., Avruch, I. M., Dutta-Roy, R., *et al.*: 2005, *Nature* **438**, 800.

Boehnhardt, H., Babion, J., and West, R. M.: 1996, *Astron. Astrophys.* **320**, 642.

Boehnhardt, H., Delahodde, C., Sekiguchi, T., Tozzi, G. P., Amestica, R., Hainaut, O., *et al.*: 2002, *Astron. Astrophys.* **387**, 1107.

Campbell, D. B., Harmon, J. K., and Shapiro, I. I.: 1989, *Astrophys. J.* **338**, 1094.

Dziak-Jankowska, B., Leliwa-Kopystynski, J., and Krolikowska, M.: 2005, Global evolution of short-period comets. 67P/Churyumov-Gerasimenko case, IAU Symp. No. 229:Asteroids, Comets, Meteors, Rio de Janeiro 2005, To apper in Earth, Moon and Planets.

Eshleman, V. R.: 1973, *Planet. Space Sci.* **21**, 1521.

Eshleman, V. R., Tyler, G. L., Anderson, J. D., Fjeldbo, G., Levy, G. S., Wood, G. E., *et al.*: 1977, *Space Sci. Rev.* **21**(2), 207.

Fjeldbo, G.: 1964, Bistatic radar methods for studying planetary ionospheres and surfaces, Stanford Electronics Laboratory, Stanford University, SU-SEL-64.

Fornasier, S., Belskaya, I., Fulchignoni, M., Barucci, M. A., and Barbieri, C.: 2006, *Astron. Astrophys.* **449**, L9.

Gill, E., Montenbruck, O., and Pätzold, M.: 1996, Perturbation forces acting on the Rosetta spacecraft in a close orbit around comet P/Wirtanen, AAS paper 96–150, Houston.

Häusler, B., Pätzold, M., Tyler, G. L., Simpson, R. A., Bird, M. K., Dehant, V., *et al.*: 2006, *Planet. Space Sci.* **54**(13–14), 1315.

Harmon, J. K., Campbell, D. B., Hine, A. A., Shapiro, I. I., and Marsden, B. G.: 1989, *Astrophys. J.* **338**, 1071.

Harmon, J. K., Ostro, S. J., Benner, L. A. M., Rosema, K. D., Jurgens, R. F., Winkler, R., *et al.*: 1997, *Science* **278**, 1921.

Howard, H. T., Eshleman, V. R., Hinson, D. P., Kliore, A. J., Lindal, G. F., Woo, R., *et al.*: 1992, *Space Sci. Rev.* **60**, 565.

Kamoun, P., Campbell, D. B., Ostro, S. J., Pettengill, G. H., and Shapiro, I. I.: 1982, *Science* **216**, 293.

Kamoun, P., Campbell, D., Pettengill, G., and Shapiro, I.: 1998, *Planet. Space Sci.* **47**, 23.

Kliore, A. J., Anderson, J. D., Armstrong, J. W., Asmar, S. W., Hamilton, C. L., Rappaport, N. J., *et al.*: 2004, *The Cassini-Huygens Mission*, Springer, The Netherlands, doi: 10.1007/1-4020-3874-7.
Konopliv, A. S., Miller, J. K., Owen, W. M., Yeomans, D. K., Giorgini, J. D., Garmier, R., *et al.*: 2002, *Icarus* **160**, 289.
Lamy, P. L., Toth, I., Weaver, H., Jorda, L., and Kaasalainen, M.: 2003, *Am. Astron. Soc. BAAS* **35**, 970.
Lazzarin, M., Marchi, S., Magrin, S., and Barbieri, C.: 2004, *Astron. Astrophys.* **425**, L25.
Lowry, S. C., Fitzsimmons, A., Jorda, L., Kaasalainen, M., Lamy, P., and Toth, I.: 2006, *Am. Astron. Soc. BAAS* **38**, 492.
Marouf, E. A., Tyler, G. L., and Eshleman, V. R.: 1982, *Icarus* 49, 161.
Marouf, E. A., Tyler, G. L., Zebker, H. A., Simpson, R. A., and Eshleman, V. R.: 1983, *Icarus*, **54**, 189.
Marouf, E. A., and Bird, M. K.: 1995, Rosetta and bistatic-radar detectability of cometary nuclei, (Abstract) AGU Fall Meeting, San Francisco, CA, December 11–15, 1995.
Marsden, B. G., and Williams, G. V.: 1995, *Catalogue of Cometary Orbits*, 10 ed., IAU Central Bureau for Astronomical Telegrams, Cambridge, MA.
Miller, J. K., Williams, B. G., Bollman, W. E., Davis, R. P., Helfrich, C. E., Scheeres, D. J., *et al.*: 1995, *J. Astronaut. Sci.* **43**, 453.
Miller, J. K., Konopliv, A. S., Antreasian, P. G., Bordi, J. J., Chesley, S., Helfrich, C. E., *et al.*: 2002, *Icarus* **155**, 3.
Mueller, B. E. A.: 1992, *Asteroids, Comets, Meteors 1991*, Lunar and Planetary Institute, Houston, p. 425.
Muhleman, D. O., and Anderson, J. D.: 1981, *Astrophys. J.* **247**, 1093.
Mysen, E., and Aksnes, K.: 2005, *Astron. Astrophys.* **443**, 691.
Mysen, E., and Aksnes, K.: 2006, *Astron. Astrophys.* **455**, 1143.
Mysen, E., Olsen, Ø., and Aksnes, K.: 2006, *Plan. Space Sci.* **54**(8), 750.
Olsen, Ø.: 2006, *Astron. Astrophys.* **449**, 821.
Ostro, S. J.: 1985, *Pub. Astron. Soc. Pacific* **97**, 877.
Ostro, S. J., Campbell, D. B., Simpson, R. A., Hudson, R. S., Chandler, J. F., Rosema, K. D., *et al.*: 1992, *J. Geophys. Res.* **97**, 18,227–18,244.
Pätzold, M., Bird, M. K., Volland, H., Edenhofer, P., and Buschert, H.: 1991a, *Z. Flugwiss. Weltraumforsch.* **15**, 89.
Pätzold, M., Bird, M. K., Volland, H., Edenhofer, P., and Buschert, H.: 1991b, *Z. Flugwiss. Weltraumforsch.* **15**, 159.
Pätzold, M., Bird, M. K., and Edenhofer, P.: 1993, *J. Geophys. Res.* **98**, 20911.
Pätzold, M., Bird, M. K., Edenhofer, P., Asmar, S. W., and McElrath, T. P.: 1995, *Geophys. Res. Lett.* **22**, 3313.
Pätzold, M., Neubauer, F. M., Andreev, V. E., and Gavrik, A. I.: 1997, *J. Geophys. Res.* **102**, 2213.
Pätzold, M., Häusler, B., Wennmacher, A., Aksnes, K., Anderson, J. D., Asmar, S. W., *et al.*: 2001a, *Astron. Astrophys.* **375**, 651.
Pätzold, M., Wennmacher, A., Häusler, B., Eidel, W., Morley, T., Thomas, N., *et al.*: 2001b, *Astron. Astrophys.* **370**, 1122.
Pätzold, M., and 21 C-Authors: 2004, MaRS: Mars Express Orbiter Radio Science, ESA-SP **1240**, 141.
Pätzold, M., and 30 Co-Authors: 2006, MaRS: the Mars Express Radio Science Experiment, ESA-SP **1291**, in press.
Richter, K., and Keller, H. U.: 1995, *Icarus* **14**, 355.
Scheeres, D. J.: 1995, *J. Astronaut. Sci.* **43**, 427.
Scheeres, D. J., Marzari, F., Tomasella, L., and Vanzani, V: 1998, *Plan. Space Sci.* **46**, 649.
Simpson, R. A., and Tyler, G. L.: 1981, *Icarus* **46**, 361.

Simpson, R. A., Tyler, G. L. Pätzold, M., and Häusler, B.: 2006, *J. Geophys. Res.* in press.
Standish, E. M.: 1993, *Astron. J.* **105**(5), 2000.
Stern, S. A., and Spencer, J.: 2003, *Moon and Planets* **92**, 477.
Tancredi, G., Fernández, J. A., Rickman, H., and Licandro, J.: 2000, *Astron. Astrophys. Suppl.* **146**, 73.
Tapley, B., Ries, J., Bettadpur, S., Chambers, D., Cheng, M., Condi, F., *et al.*: 2005, "GGM02 – An improved Earth gravity field model from GRACE," *Journal of Geodesy*, DOI 10.1007/s00190–005-0480-z.
Tyler, G. L.: 1968, *J. Geophys. Res.* **73**, 7609.
Tyler, G. L.: 1987, Radio propagation experiments in the outer solar system with Voyager, *Proceedings of the IEEE* **75**(10), 1404.
Tyler, G. L., Eshleman, V. R., Fjeldbo, G., Howard, H. T., and Peterson, A. M.: 1967*Science*, **157**(3785), 193.
Tyler, G. L., and Howard, H. T.: 1973, *J. Geophys. Res.* **78**, 4852.
Tyler, G. L., Marouf, E. A., Simpson, R. A., Zebker, H. A., and Eshleman, V. R.: 1983, *Icarus*, **54**, 160.
Tyler, G. L.: 1987, Radio propagation experiments in the outer solar system with Voyager, *Proceedings of the IEEE* **75**, 1404.
Tyler, G. L., Balmino, G., Hinson, D. P., Sjogren, W. L., Smith, D. E., Woo, R., *et al.*: 1992, *J. Geophys. Res.* **97**, 7759.
Tyler, G. L., Simpson, R. A., Maurer, M. J., and Holmann, E.: 1992, *J. Geophys. Res.* **97**, 13115.
Yakovlev, O. I., and Efimov, A. I.: 1966, *Dokladi Akademii Nauk SSSR* **174**, 583.
Yeomans, D. K.: 1986, Physical interpretations from the motions of comets Halley and Giacobini-Zinner, ESA SP-250 II, p. 419.
Yeomans, D. K., Ananda, M., Sjogren, W. L., and Wood, L. J.: 1981, *J. Astronautical Sci.* **29**, 19.
Yeomans, D. K., Barriot, J.-P., Dunham, D. W., Farquhar, R. W., Giorgini, J. D., Helfrich, C. E., *et al.*: 1997, *Science* **278**, 2106.
Von Oertzen, J.: 2003, Global modelling of comets: Nucleus, neutral and ionized coma of comets 67P/Churyumov-Gerasimenko and 46 P/Wirtanen, Mitteilungen aus dem Institut für Geophysik und Meteorologie Heft 156, Köln.